Observational Consequences of Angular Momentum in Fission

R. Vogt[1,2,*] and *J.* Randrup[3]

[1]Nuclear and Chemical Sciences Division, Lawrence Livermore National Laboratory, Livermore, CA, USA
[2]Physics and Astronomy Department, University of California, Davis, CA, USA
[3]Nuclear Science Division, Lawrence Berkeley National Laboratory, Berkeley, CA, USA

Abstract. The role of angular momentum in fission has been the subject of intense recent attention. Published data showed that, while the fission fragment spins may be generated by highly correlated processes, the final, measured, fragment spins appeared to be largely uncorrelated. Advances made with the fission simulation model FREYA to study the role of angular momentum in fission are summarized. It is shown that FREYA can simulate a variety of scenarios for generating fragment spin and determine the observational consequences.

1 Background

Nuclear fission has been intensely studied for more than 80 years. While much is known about certain aspects related to applications, others have yet to be understood in detail. Phenomenological models that describe fission event-by-event are useful for studying potentially correlated observables. The complete fission model FREYA is particularly ideal for studies related to angular momentum because it conserves both linear and angular momentum.

The first studies of angular momentum in fission were in the 1970s. The classic early measurements of photon angular distributions relative to the fragment motion [1, 2] suggested that the angular momentum of the primary fragments were perpendicular to the fission axis, although with large uncertainties. While other, more recent experiments, studied neutron-photon correlations [3–5] or the dependence of photon emission on fragment mass and total kinetic energy [3, 6, 7], there were no direct experimental follow ups of the original studies on angular momenta [1, 2]. However, Ref. [8] recently studied fragment spin correlations based on rotational transitions [8] and found that the average spin of one fragment was practically independent of the minimum spin of the other fragment. Based on this finding, they concluded that there was no significant correlation between the fragment spins and the fragment spins must be generated after scission, after the fragments have become two separate, independent systems [8], in apparent violation of angular momentum conservation.

FREYA calculations show that, even though the fragment spins begin as highly correlated, the population of both positive and negative rotational modes decorrelates the spins. Here FREYA is introduced and the character of these modes are discussed, along with how studies of photon angular distributions can determine the relative excitation of these modes.

*e-mail: rlvogt@lbl.gov

2 Generating Fission Events with FREYA

FREYA requires the mass distribution of the primary fission fragments, $Y(A)$, and the mean total kinetic energy for a given mass split, $\overline{\mathrm{TKE}}(A)$. However, FREYA can also be configured to accept the yields in other forms [9, 10].

Assuming binary fission, the compound nucleus A_0 splits into light and heavy fragments, A_L and A_H. The first fragment is sampled from $Y(A)$ and its partner fragment is then determined by mass and charge conservation. The fission Q-value is calculated from the mass excess and the average TKE is taken from $\mathrm{TKE}(A_H)$. Energy conservation is used to obtain the total excitation energy available for rotational and statistical excitation at scission, $E^*_{\rm sc} = Q - \overline{\mathrm{TKE}}$. The 'scission temperature' $T_{\rm sc}$ is obtained from $E^*_{\rm sc} = a(A_0)T^2_{\rm sc}$ with the level density parameter $a(A) \propto A/e_0$ where $e_0 \approx 10$ MeV.

The overall rigid rotation of the fissioning system determines the mean fragment angular momenta. However, fluctuations around these mean values arise due to agitation of the wriggling and bending angular momentum modes in the default version of FREYA, as discussed in Sec. 3. Assuming these modes are fully excited, the magnitude of these spin fluctuations is determined by a 'spin temperature' $T_S = c_S T_{\rm sc}$ with parameter c_S. In Sec. 4, the possible agitation of the twisting mode is also considered and a value of c_S is individually assigned to each mode.

After subtracting the rotational energy of the fragments, $E_{\rm rot}$, from the total available excitation energy, $E_{\rm stat} = E^*_{\rm sc} - E_{\rm rot}$ is left for statistical excitation. It is partitioned between the fragments based on their heat capacities and a parameter x that provides additional excitation energy to the light fragment.

Once the mean fragment excitation energies have been so determined, FREYA considers thermal fluctuations of $E_{\rm stat}$. The energy fluctuation δE^*_i is sampled from a truncated Gaussian with variance $2c\overline{E}^*_i T_i$. The fragment excitation energies are consequently adjusted, $E^*_i = \overline{E}^*_i + \delta E^*_i$,

$i = L, H$. with overall energy conservation enforced by introducing a compensating fluctuation in TKE, TKE = $\overline{\text{TKE}} - \delta E_L^* - \delta E_H^*$. Finally, TKE is adjusted by the parameter dTKE, to reproduce the average neutron multiplicity.

After the fragment initial conditions have been fixed, neutrons and photons are emitted. Neutrons are emitted statistically (according to $\epsilon_n \exp(-\epsilon_n/T)$) [11]. The emission is isotropic in the frame of the emitter fragment, apart from a slight flattening due to the rotation of the fragment. Neutron evaporation continues until the fragment excitation energy is below the neutron separation energy S_n.

After neutron evaporation ends, photons are emitted. First, statistical photons are emitted isotropically with an energy distribution, $\epsilon_\gamma^2 \exp(-\epsilon_\gamma/T)$, modulated by a giant-dipole resonance form factor [12]. When the remaining nuclear excitation energy is in the range of RIPL-3 compilation [13], `FREYA` switches to a discrete cascade that continues until the half-life of the state exceeds a specified value, $t_{\max}$, based on the detector response time, or until the nucleus is in its ground state.

The `FREYA` parameters described here: e_0, c_S, x, c and dTKE have tuned to data for the nuclei in `FREYA` that spontaneously fission [14]. While there are well measured data on ^{252}Cf(sf), the data for the other cases are typically more sparse, especially for ^{238,240,242}Pu(sf) where generally only an evaluation of $\overline{\nu}$ and its moments are available [14]. The very small uncertainties on the evaluation [15] placed tight constraints on c without constraining the other parameters. More data are now available for the prompt fission neutron spectrum of ^{240}Pu(sf) [16, 17] and more new measurements may become available. Thus, these isotopes are being given another look, perhaps leading to better overall constraints on all the `FREYA` parameters for these isotopes.

3 Dinuclear rotational modes

As the system approaches scission, two proto-fragments in close proximity emerge with nucleon numbers, (Z_L, N_L) and (Z_H, N_H), frozen in. These proto-fragments are in relative motion with angular momentum $\boldsymbol{L} = \boldsymbol{R} \times \boldsymbol{P}$ where $\boldsymbol{R} \equiv \boldsymbol{R}_L - \boldsymbol{R}_H$ is the relative position of the light and heavy proto-fragments. The direction of $\boldsymbol{R}$ at scission defines the fission axis. The relative fragment momentum is $\boldsymbol{P} = \mu(\boldsymbol{V}_L - \boldsymbol{V}_H)$ with fragment velocity $\boldsymbol{V}_i$ and reduced fragment mass $\mu \approx mA_LA_H/(A_L + A_H)$. The proto-fragments also generally have angular momenta, $\boldsymbol{S}_L$ and $\boldsymbol{S}_H$, with a total, conserved, angular momentum of $\boldsymbol{S}_0 = \boldsymbol{S}_L + \boldsymbol{S}_H + \boldsymbol{L}$. The fissioning system undergoes overall rigid rotation with angular momentum $\boldsymbol{S_0}$. Note that $\boldsymbol{S_0}$ is negligible for low energy induced fission and absent in spontaneous fission.

The angular-momentum modes can be rewritten in normal form [18–20] as

$$E_0^{\text{rot}} = \frac{S_L^2}{2\mathcal{I}_L} + \frac{S_H^2}{2\mathcal{I}_H} + \frac{(\boldsymbol{S}_0 - \boldsymbol{S}_L - \boldsymbol{S}_H)^2}{2\mathcal{I}_R} \quad (1)$$
$$= \frac{S_0^2}{2\mathcal{I}_0} + \frac{s_{\text{wrig}}^2}{2\mathcal{I}_{\text{wrig}}} + \frac{s_{\text{bend}}^2}{2\mathcal{I}_{\text{bend}}} + \frac{s_{\text{twst}}^2}{2\mathcal{I}_{\text{twst}}} + \frac{s_{\text{tilt}}^2}{2\mathcal{I}_{\text{tilt}}}$$

where $\mathcal{I}_L$ and $\mathcal{I}_H$ are the fragment moments of inertia $\mathcal{I}_R = \mu R^2$ is the moment of inertia for the orbital motion, and $\mathcal{I}_0 = \mathcal{I}_L + \mathcal{I}_H + \mathcal{I}_R$ is the total moment of inertia. The normal modes: wriggling, bending, twisting and tilting [18] are now discussed.

The rotational energy is minimized when none of the normal modes are agitated, leaving only rigid rotation. The normal modes, which carry no net angular momentum, make fluctuating contributions in addition to rigid rotation. The wriggling and bending modes, which are assumed to be fully agitated in default `FREYA`, are perpendicular to the fission axis. The twisting and tilting modes are parallel to the fission axis. The contributions of the fluctuations dominate over rigid rotation [21].

The wriggling contributions, perpendicular to $\boldsymbol{R}$, the fission axis, are parallel to each other,

$$\delta\boldsymbol{S}_{L,H}^{\text{wrig}} = ((\mathcal{I}_{L,H})/(\mathcal{I}_L + \mathcal{I}_H))\boldsymbol{s}_{\text{wrig}}\,, \quad \delta\boldsymbol{L}^{\text{wrig}} = -\boldsymbol{s}_{\text{wrig}}\,, \quad (2)$$

with $\mathcal{I}_{\text{wrig}} = (\mathcal{I}_L + \mathcal{I}_H)\mathcal{I}_R/\mathcal{I}_0$ in Eq. (1). The change in $\boldsymbol{L}$, required to conserve angular momentum, also reduces the moment of inertia by $\mathcal{I}_R/\mathcal{I}_0$. Because the space perpendicular to $\boldsymbol{R}$ is two dimensional, there are two independent, degenerate wriggling modes.

The bending contributions, also perpendicular to $\boldsymbol{R}$, are anti-parallel to each other,

$$\delta\boldsymbol{S}_L^{\text{bend}} = \boldsymbol{s}_{\text{bend}}\,, \quad \delta\boldsymbol{S}_H^{\text{bend}} = -\boldsymbol{s}_{\text{bend}}\,, \quad \delta\boldsymbol{L}^{\text{bend}} = \boldsymbol{0}\,, \quad (3)$$

with $\mathcal{I}_{\text{bend}} = \mathcal{I}_L\mathcal{I}_R/(\mathcal{I}_L + \mathcal{I}_R)$ in Eq. (1). Because the bending contributions to the spins are equal and opposite, bending has no effect on $\boldsymbol{L}$. Like wriggling, the bending modes are independent and degenerate.

The twisting contributions are parallel to $\boldsymbol{R}$ and opposite, $\boldsymbol{s}_{\text{twst}} = s_{\text{twst}}\hat{\boldsymbol{R}}$,

$$\delta\boldsymbol{S}_L^{\text{twst}} = \boldsymbol{s}_{\text{twst}}\,, \quad \delta\boldsymbol{S}_H^{\text{twst}} = -\boldsymbol{s}_{\text{twst}}\,, \quad \delta\boldsymbol{L}^{\text{twst}} = \boldsymbol{0}\,, \quad (4)$$

with $\mathcal{I}_{\text{twst}} = \mathcal{I}_{\text{bend}}$ in Eq. (1).

In the tilting mode, the spins are also parallel to $\boldsymbol{R}$, $\boldsymbol{s}_{\text{tilt}} = s_{\text{tilt}}\hat{\boldsymbol{R}}$,

$$\delta\boldsymbol{S}_i^{\text{tilt}} = (\mathcal{I}_i/\mathcal{I}_{\text{tilt}})\boldsymbol{s}_{\text{tilt}}\,, \quad \delta\boldsymbol{L}^{\text{tilt}} = -\boldsymbol{s}_{\text{tilt}}\,, \quad (5)$$

with $\mathcal{I}_{\text{tilt}} = \mathcal{I}_L + \mathcal{I}_H$ in Eq. (1). In an isolated system, such as this, tilting is not directly excited but appears only because the orbital plane of motion is tilted in response to wriggling recoils perpendicular to $\boldsymbol{L}$. The tilting time scale is therefore long [20] so that it can be ignored.

The proto-fragment angular momenta is built from contributions of the normal rotational modes. In these modes, the two spins are highly correlated. In the thermal limit, the modes are populated statistically. Thus the distribution of spin fluctuations of mode m are $P_m(s_m) \sim \exp(-s_m^2/2\mathcal{I}_m T)$, giving a corresponding variance of $\langle s_m^2\rangle_T = \mathcal{I}_m T$, where T is the effective temperature [19]. Whether or not the statistical limit is reached depends on the characteristic time scales for their excitation.

Each mode has a relaxation time, t_m, its equilibration time scale. If t_m is significantly shorter than the fission time, the mode should be in equilibrium at scission. If t_m is similar to or longer than the fission time, it is not. The rotational time scales were derived based on the nucleon

exchange transport model [22, 23]. Although it was developed to understand the dynamical evolution of damped nuclear reactions [24, 25], the basic physics can equally well apply to the fissioning system prior to fission, when the binary proto-fragments have been formed.

The relaxation time for mode m is $t_m = \mathcal{I}_m/M_m$, where $\mathcal{I}_m$ is the moment of inertia of the mode and M_m is its mobility coefficient, derived [20] based on the nucleon exchange transport model [23],

$$M_{\rm wrig} = m\mathcal{N}R^2 , \quad (6)$$

$$M_{\rm bend} = m\mathcal{N}\left[\left(\frac{\mathcal{I}_H R_L - \mathcal{I}_L R_H}{\mathcal{I}_L + \mathcal{I}_H}\right)^2 + c^2_{\rm ave}\right] , \quad (7)$$

$$M_{\rm twst} = m\mathcal{N}c^2_{\rm ave} . \quad (8)$$

The rate at which nucleons transfer between fragments is given by $\mathcal{N} \approx \frac{1}{4}\rho\bar{v}\pi c^2$ [26] where ρ is the nucleon density, $\bar{v} = \frac{3}{4}v_F$ is the mean nucleon speed, $c^2_{\rm ave} = \frac{1}{2}c^2$ is the average value of the neck radius c squared, and $R = R_L + R_H + 4$ fm. $M_{\rm twst}$ is an order of magnitude smaller than $M_{\rm wrig}$ because $R^2 \gg c^2$, giving $t_{\rm twst} \gg t_{\rm wrig}$. The first term in $M_{\rm bend}$ vanishes for symmetric splits, giving $M_{\rm bend} = M_{\rm twst}$. $M_{\rm bend}$ is significantly larger than $M_{\rm twst}$ for typical asymmetric mass splits and small c. The relaxation times as a function of c are shown in Fig. 1.

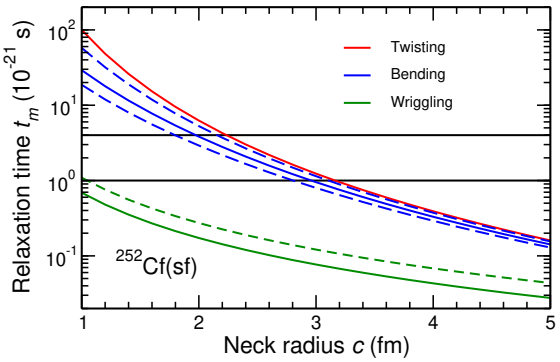

Figure 1. The calculated relaxation times t_m for wriggling (bottom curve, green), bending (middle three curves, blue), and twisting (top curve, red), shown as functions of the neck radius c for $d = 4$ fm. The wriggling result is also shown for touching spheres, $d = 0$ (dashed green). The bending curves show the most probable mass split (108:144, solid) and two 50% probable splits (100:152, lower dashed, and 118:134, upper dashed). The horizontal lines show $t_{\rm fiss} = 1$ and $t_{\rm fiss} = 4 \times 10^{-21}$ s.

The relaxation times are compared with $t_{\rm fiss}$, the time needed for the fissioning system to evolve from the time the proto-fragments first appear to the neck rupture. Because $t_{\rm fiss}$is difficult to measure experimentally, it is not well known [27].Here $t_{\rm fiss}$ is assumed to be between one to a few 10^{-21} s. As seen in Fig. 1, $t_{\rm wrig}$ is well below $t_{\rm fiss}$so that the wriggling mode is likely to stay equilibrated until the scission time when $c \approx 2$ fm.

On the other hand, $t_{\rm twst}$ is similar to or longer than $t_{\rm fiss}$. If the rotational modes are not strongly agitated, as in spontaneous fission, twisting may not be built up prior to scission. Twisting should become more important for induced fission at higher excitation energies.

The contribution due to bending is more difficult to predict without a more precise estimate of $t_{\rm fiss}$. However, if $c \approx 2$ fm and $t_{\rm fiss}$ is several times 10^{-21} s, bending may have some appreciable agitation. The results in Wilson *et al.* [8] suggest that the spin magnitudes of the fragments are fairly independent, limiting suppression of the bending mode. Because the bending contribution increases with the mass asymmetry, see Eq. (7), its contribution could be studied as a function of the mass yields.

Based on these calculations, the wriggling modes should be fully equilibrated at scission while bending should be partially, if not fully, equilibrated. Twisting may be present but its contribution is less significant.

4 Simulating angular momentum modes

The angular momentum treatment described here has been incorporated into `FREYA` [28–30]. At scission, each of the normal modes m is sampled from a Boltzmann distribution with effective temperature $T_m = c_m T_{\rm sc}$. Thus the distribution of mode amplitudes s_m is $P(s_m) \sim \exp(-s_m^2/2\mathcal{I}_m T_m)$ with $c_m = (c_{\rm wrig}, c_{\rm bend}, c_{\rm twst})$. The default version of `FREYA` uses $c_S = c_m = (1, 1, 0)$ [29, 30]. In this discussion, the coefficients c_m adjusted individually to explore different degrees of agitation. Note than when values of c_m other than the default are employed, the coefficients are renormalized to ensure that the average fragment spin magnitudes remain the same.

After scission, the primary fission fragments separate along Coulomb trajectories. The associated rotation of the dinuclear axis $\boldsymbol{R} \equiv \boldsymbol{R}_L - \boldsymbol{R}_H$ is very small, is only a couple of degrees [30]. Thus the fragments move approximately along the fission axis. As they separate, each fragment evaporates neutrons and photons, as described in Sec. 2.

Photon radiation is emphasized with a simplified description to enhance the physical effects discussed here. If these turn out to be sufficiently promising to warrant experimental investigations, more refined treatments should be developed.

`FREYA` treats neutron evaporation classically, leaving the product nucleus with a spin vector $\boldsymbol{S}$. Here the spin magnitude, $S \equiv |\boldsymbol{S}|$, is replaced by a discrete integer or half-integer value J according to whether the mass number A of the product (after neutron evaporation) is even or odd. Further, it is assumed that the post-evaporation fission product is in a quantum state maximally aligned along the spin direction $\hat{\boldsymbol{S}}$. Then the initial state, before the photon cascade begins, is given by $|i\rangle = |J, M = J\rangle$ when $\hat{\boldsymbol{S}}$ is the quantization axis.

In its ground state, the product nucleus angular momentum may be directed along its symmetry axis with magnitude $K_{\rm gs}$. The possible values of J are $J = K_{\rm gs}, K_{\rm gs} + 1, \ldots$ with associated rotational energy

$$E_{\rm rot} = [J(J+1) - K_{\rm gs}(K_{\rm gs}+1)]/\mathcal{I}_\perp(A) , \quad (9)$$

vanishing in the ground state, $E^{\rm gs}_{\rm rot} = 0$. The moment of inertia is assumed to be 50% of its rigid value for simplicity,

$\mathcal{I}_\perp(A) = 0.5\times\frac{2}{5}mAR_A^2$. The statistical excitation energy of the product nucleus is $E_{\rm stat} = E_{\rm tot} - E_{\rm rot}$, where $E_{\rm tot}$ denotes the total excitation of the mother state. As in the standard FREYA treatment, the nucleus is assumed to first dispose of its statistical excitation energy through a sequence of E1 dipole photon emissions, The simulation of the E1 cascades is carried out with a recently developed semi-classical method [31] that replaces the daughter state with a state that is also maximally aligned but along a direction that may be tilted relative to that of the mother state. The E1 cascades continue until the nucleus has reached the yrast line. For even-even nuclei, $K_{\rm gs}$ vanishes and the yrast states only have even J values, $J = 0, 2, 4\ldots$.

As should be clear from the previous discussion, the spins of the two fragments are not independent because angular momentum is conserved. The spin contributions from the two fragments due to wriggling are perfectly parallel, while the contributions from bending are anti-parallel. When these modes are populated statistically, the correlation coefficient for the individual fragment spins is $c(\boldsymbol{S}_L, \boldsymbol{S}_H) \equiv [\langle \boldsymbol{S}_L\cdot\boldsymbol{S}_H\rangle - \langle \boldsymbol{S}_L\rangle\langle \boldsymbol{S}_H\rangle]/[\sigma_L\sigma_H] = -\{\mathcal{I}_L\mathcal{I}_H/[(\mathcal{I}_R+\mathcal{I}_L)(\mathcal{I}_R+\mathcal{I}_H)]\}^{1/2}$. Because the moment of inertia of relative fragment motion, $\mathcal{I}_R$, is typically an order of magnitude larger than $\mathcal{I}_L$ and $\mathcal{I}_H$, $\mathcal{I}_R \gg \mathcal{I}_f$, $c(\boldsymbol{S}_L, \boldsymbol{S}_H)$ is rather small. Thus, even though the fragment spins are strongly coupled for each of the normal modes, the resulting spins are relatively independent, as is shown by FREYA calculations [21, 32] and in accord with Ref. [8].

5 Angular distribution of E2 photons

Here sequential emission of collective E2 photons along the ground-state band in even-even product nuclei is studied. In such processes, when the mother state is maximally aligned, the daughter state is also maximally aligned. Thus photon emission does not change the directional alignment of the spin but only reduces its magnitude by $2\hbar$. All photons emitted in each collective cascade are uncorrelated with the same angular distribution.

The angular distribution of a photon emitted from a maximally aligned state $|J, J\rangle$ can be expressed in polar coordinates (θ, ϕ) relative to the quantization axis (spin direction). The distribution is azimuthally symmetric around the spin direction so that the distribution of stretched E2 transitions as a function of θ is

$$P^2_{2,h}(\theta) \;=\; \tfrac{5}{2}\left(d^2_{2,h}(\theta)\right)^2 \;=\; \tfrac{5}{8}(1 + h\cos\theta)^2\sin^2\theta\,, \quad (10)$$

where $d^2_{2,h}(\theta)$ is a Wigner d-function and h is the photon helicity. The distribution is normalized so that $\int P^2_{2,h}(\theta)\, d\cos\theta = 1$.

The angular distribution of collective photons is studied relative to the direction of motion of the fission product that emits them: photons emitted from the light product are measured relative to the light product direction while photons emitted from the heavy product are measured relative to its direction. In an actual experiment, one or both of the product nuclei may not be detected. However, because the two fragments move in nearly opposite directions, it is possible to tell which product nucleus emitted the photon.

The study focuses on even-even product nuclei with specific E2 transitions that stand out sufficiently clearly above the background. FREYA can include all collective photons emitted during de-excitation of the selected product nuclei. While this is not possible experimentally because not all transitions can be identified or detected, this is not prohibitive because the signal from each identified E2 transition, and from all such nuclei, is additive. Therefore, the angular distributions are averaged over all collective transitions, automatically taking into account the increased intensity of the lower transitions.

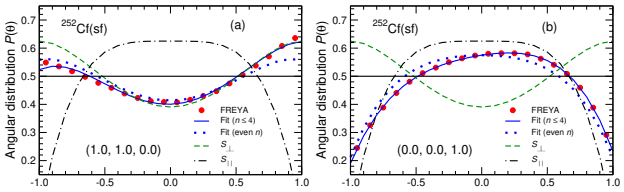

Figure 2. The angular distribution of collective E2 photons relative to the direction of the emitting product nucleus for standard FREYA, where only the wriggling and bending modes are fully agitated (a) and one where only twisting is present (b). The values of $(c_{\rm wrig}, c_{\rm bend}, c_{\rm twst})$ are indicated. The Legendre fits (solid curves) and their symmetric parts (dots) are shown, as are $P_\parallel(\theta_{\gamma,f})$ and $P_\perp(\theta_{\gamma,f})$. From Ref. [33].

This distribution is especially interesting because it is sensitive to the direction of the angular momentum of the emitting nucleus. The angular momenta of the primary fragments are predicted to be nearly perpendicular to the fission axis at the time of scission, $\hat{\boldsymbol{R}}(t_{\rm sciss})$ as is also suggested by experiment [1, 2]. However, even if the spins were originally exactly perpendicular to $\hat{\boldsymbol{R}}(t_{\rm sciss})$, they would not be perpendicular to the direction of the asymptotic fragment motion due to recoils from the evaporated neutrons and statistical (E1) photon emission, as well as the slight Coulomb rotation [34]. The correlations between the fragment spins can change considerably whether the fragment spins emerge perpendicular to the fission axis, as assumed in standard FREYA, or whether they are independent of the fission axis, see Ref. [35].

Figure 2 shows the angular distribution $dN/d\cos\theta_{\gamma,f}$ for two opposite assumptions about the excitation of the rotational modes, obtained by specifying the parameters $\{c_m\}$ in FREYA. For reference, the idealized distributions $P_\parallel(\theta_{\gamma,f})$ and $P_\perp(\theta_{\gamma,f})$ are shown in each case. While $P_\parallel(\theta_{\gamma,f})$ and $P_\perp(\theta_{\gamma,f})$ are symmetric around 90°, the simulated distributions are forward skewed by the motion of the emitting fragment relative to the laboratory frame. Because the fragment velocities are rather small, it is possible to correct for this focusing effect.

Figure 2(a) shows the standard FREYA scenario where both the wriggling and bending modes are fully excited. Because the spins of these modes are perpendicular to the fission axis, the distribution is similar to $P_\perp(\theta_{\gamma,f})$. The difference is due to dealignment of the spin caused by prior emissions. This scenario is consistent with the data in Refs. [1, 2], albeit with large uncertainties.

A less realistic scenario is shown in Fig. 2(b). Here only twisting is fully agitated, resulting in an oblate angular distribution, similar to $P_{\|}(\theta_{\gamma,f})$.

It may be possible to determine the degree of twisting employing the yield ratio, $W(0°):W(90°)$, the forward relative to the sidewards yields, as illustrated in Fig. 3. The yield ratio is shown as a function of the coefficient of the twisting mode, $c_{\rm twst}$. There is a nearly linear decrease as $c_{\rm twst}$ increases. Even the apparent small change in $dN/d\cos\theta$ in Figs. 2(a) and (b), from $c_{\rm twst} = 0$ to 0.2 results in a significant decrease in $W(0°) : W(90°)$. It is worth noting that even though $W(0°):W(90°)$ is quite sensitive to $c_{\rm twst}$, it is effectively independent of the relative proportion of wriggling and bending: the results for three very different values of $c_{\rm bend}:c_{\rm wrig}$ are nearly identical.

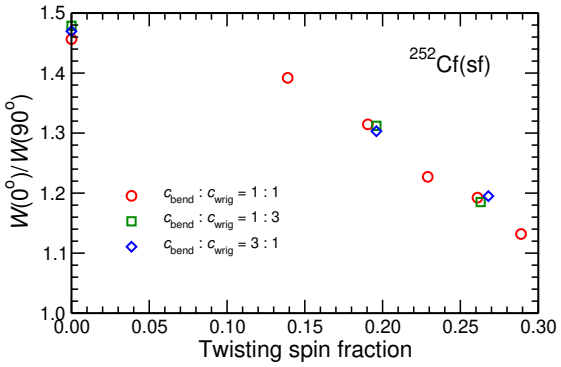

Figure 3. $W(0°):W(90°)$ as a function of $c_{\rm twst}$. From Ref. [33].

This work was performed under the auspices of the U.S. Department of Energy by LBNL under Contract DE-AC02-05CH11231 (JR) and LLNL under Contract DE-AC52-07NA27344 (RV).

References

[1] J. B. Wilhelmy et al., Phys. Rev. C **5**, 2041 (1972). doi:10.1103/PhysRevC.5.2041
[2] A. Wolf and E. Cheifetz, Phys. Rev. C **13**, 1952 (1976). doi:10.1103/PhysRevC.13.1952
[3] T. Wang et al., Phys. Rev. C **93**, 014606 (2016). doi:10.1103/PhysRevC.93.014606
[4] S. Marin et al., Phys. Rev. C **104**, 024602 (2021). doi:10.1103/PhysRevC.104.024602
[5] S. Marin et al., Phys. Rev. C **105**, 054609 (2022). doi:10.1103/PhysRevC.105.054609.
[6] A. Al-Adili et al., EPJ Web Conf. **256**, 00002 (2021). doi.org/10.1051/epjconf/202125600002
[7] M. Travar et al., Phys. Lett. B **817**, 136293 (2021). doi:10.1016/j.physletb.2021.136293
[8] J. Wilson et al., Nature **590**, 566 (2021). doi:10.1038/s41586-021-03304-w
[9] J. Randrup, P. Talou and R. Vogt, Phys. Rev. C **99**, 054619 (2019). doi:10.1103/PhysRevC.99.054619
[10] N. Vassh et al., J. Phys. G **46**, 065202 (2019). doi:10.1088/1361-6471/ab0bea
[11] J. Randrup and R. Vogt, Phys. Rev. C **80**, 024601 (2009) .doi:10.1103/PhysRevC.80.024601
[12] R. Vogt and J. Randrup, Phys. Rev. C **96**, 064620 (2017). doi:10.1103/PhysRevC.96.064620
[13] R. Capote et al., Nucl. Data Sheets **110**, 3107 (2009). doi:10.1016/j.nds.2009.10.004
[14] J. Van Dyke, L. Bernstein and R. Vogt, Nucl. Instrum. Meth. A **922**, 36 (2019). doi:10.1016/j.nima.2019.01.001
[15] P. Santi and M. Miller, Nucl. Sci. Eng. **160**, 190 (2008). doi.org/10.13182/NSE07-85
[16] B. Gerasimenko et al., J. Nucl. Sci. Technol. **39**, 362 (2002). doi:10.1080/00223131.2002.10875115
[17] K. Kelly et al., Phys. Rev. C **109**, 064611 (2024). doi.org/10.1103/PhysRevC.109.064611
[18] J. R. Nix and W. J. Swiatecki, Nucl. Phys. **71**, 1 (1963). doi.org/10.1016/0029-5582(65)90038-
[19] L. G. Moretto and R. P. Schmitt, Phys. Rev. C **21**, 204 (1980). doi:10.1103/PhysRevC.21.204
[20] T. Døssing and J. Randrup, Nucl. Phys. A **433**, 215 (1985). doi:10.1016/0375-9474(85)90178-2
[21] J. Randrup and R. Vogt, Phys. Rev. Lett. **127**, 062502 (2021). doi:10.1103/PhysRevLett.127.062502
[22] J. Randrup, Nucl. Phys. A **327**, 490 (1979). doi:10.1016/0375-9474(79)90271-9
[23] J. Randrup, Nucl. Phys. A **383**, 468 (1982). doi:10.1016/0375-9474(82)90087-2
[24] W. U. Schröder et al., Phys. Rev. Lett. **44**, 308 (1980). doi.org/10.1103/PhysRevLett.44.308
[25] W. U. Schröder and J. P. Huizenga, in Treatise On Heavy-Ion Science, ed. D.A. Bromley (Plenum, New York, 1984), p. 115. www.osti.gov/biblio/5868988
[26] J. Błocki et al., Ann. Phys. **113**, 330 (1978). doi:10.1016/0003-4916(78)90208-7
[27] B. B. Back, JPS Conf. Proc. 32, 0100002 (2020). doi:10.7566/JPSCP.32.010002
[28] J. M. Verbeke, J. Randrup, and R. Vogt, Comp. Phys. Comm. **191**, 178 (2015). doi:10.1016/j.cpc.2015.02.002
[29] J. M. Verbeke, J. Randrup, and R. Vogt, Comp. Phys. Comm. **222**, 263 (2018). doi.org/10.17632/2mssy7r3gt.1
[30] J. Randrup and R. Vogt, Phys. Rev. C **89**, 044601 (2014). doi:10.1103/PhysRevC.89.044601
[31] J. Randrup and T. Døssing, Phys. Rev. C **109**, 054613 (2024). doi:10.1103/PhysRevC.109.054613
[32] R. Vogt and J. Randrup, Phys. Rev. C **103**, 014610 (2021). doi:10.1103/PhysRevC.103.014610
[33] J. Randrup, T. Døssing and R. Vogt, Phys. Rev. C **106**, 014609 (2022). doi:10.1103/PhysRevC.106.014609
[34] J. Randrup, Phys. Rev. C **108**, 064606 (2023). doi:10.1103/PhysRevC.108.064606
[35] J. Randrup, Phys. Rev. C **106**, L051601 (2022). doi.org/10.1103/PhysRevC.106.L051601